An Ultra-Wideband Microwave Photonic Channelized Receiver with Zero-IF Architecture

Bo Chen [1,2]**, Yangyu Fan** [1]**, Zhou Tian** [3]**, Wuying Wang** [1]**, Bochao Kang** [1]**, Wei Jiang** [3] **and Yongsheng Gao** [1,]*

[1] School of Electronics and Information, Northwestern Polytechnical University, Xi'an 710129, China; chen_bo_16@163.com (B.C.); fan_yangyu@nwpu.edu.cn (Y.F.); mynaw@163.com (W.W.); kangbochao1989@163.com (B.K.)
[2] School of Physics & Electronic Engineering, Xianyang Normal University, Xianyang 712000, China
[3] China Academy of Space Technology, Xi'an 710100, China; tianz@504cast.com (Z.T.); tsingh504@163.com (W.J.)
* Correspondence: ysgao@nwpu.edu.cn; Tel.: +86-181-9219-0520

check for updates

Abstract: A scheme for realizing a zero-intermediate frequency (IF) channelized receiver using a dual-polarization quadrature phase-shift keying (DP-QPSK) modulator and a narrow-band optical filter is proposed. The channelized system only requires one optical frequency comb to achieve zero-IF multi-channel reception of wideband signals, and the spacing of the optical frequency comb only needs to be equal to the sub-channel width, which is very easy to implement. It is found that using photonic IQ demodulation and balanced detection and reception technology can not only eliminate many disadvantages of the traditional zero-IF receiver, including local oscillator (LO) leakage, direct current (DC) offset, even-order distortion, and in-phase/quadrature (I/Q) imbalance, but also reduce the bandwidth and sample rate of the analog-to-digital converter (ADC). It is theoretically proven that the radio frequency (RF) signal with a bandwidth of 3 GHz can be divided into five sub-channels with a bandwidth of 600 MHz and finally demodulated to I/Q basebands, which are also verified with simulation.

Keywords: microwave photonic channelization; balanced detection; zero-intermediate frequency (IF) receiver; IQ demodulation

1. Introduction

The receiving technology of ultra-wideband (UWB) radio frequency signal has always been a research hotspot in the field of communication. For example, the radar system or electronic warfare needs to process multiple signals of different frequencies arriving at the same time in real time, which can be achieved through a channelized receiver by segmenting the electromagnetic spectrum, so as to realize the full probability interception of signals in the monitoring range of the UWB. Another example is the application in navigation or wireless communications, where it greatly improves the bandwidth efficiency of the wireless communication. So, the channelized receiver can be well applied to photonic technology for 5G. A channelized receiver is usually required to have a broad instantaneous receiving bandwidth, a high resolution, and a high sensitivity, guaranteeing signal processing; it can also process signals at multiple frequency points and various forms of signals at the same time, and has a high resolution and sensitivity [1,2]. However, the current analog-to-digital converters (ADCs) are limited by sampling rates and bandwidths, which cannot simultaneously process ultra-wideband signals [3]. A channelized receiver can slice the received broadband radio frequency (RF) signal into multiple sub-bands and down-convert each sub-band to the common intermediate frequency

(IF) or zero intermediate frequency (zero-IF). The zero-IF receiving structure used in this scheme has the following advantages. It can directly down-convert RF signals to baseband signals, which simplifies the system structure, not only reducing the system volume, but also the cost. In addition, it reduces the bandwidth requirements for ADCs and enhances the digital processing capability of broad instantaneous bandwidth signals.

The traditional analog channelized receiver has large power consumption, large insertion loss, high requirements on the electrical filter, and also a large bulk when the number of sub-channels increases, which is gradually replaced by digital channelized receivers. The digital receiver has flexible tunability and high accuracy but is also limited by the sampling rate of the ADC and working bandwidth [4]. In electronic warfare, massive amounts of data also place higher demands on signal processing. So, it is urgent to develop a channelized receiver that can process ultra-wideband signals [5].

In recent years, microwave photonic technology has developed rapidly. Owing to the wide instantaneous bandwidth, broad working frequency range, high isolation, and immunity to electromagnetic interference (EMI), it provides a new solution for the realization of a channelized receiver. A continuous light wave generated by a laser diode (LD) is used as a carrier wave to modulate the RF signals to transmit. The entire transmission link is almost the optical link, and the entire system also uses optical components. For example, optical fibers have replaced cables and optical filters have replaced electrical filters. The optical signals are not transformed to electrical signals before the balanced photodiode (BPD). Since it meets the current demand for large bandwidth in many fields, the channelized receiver based on photonics has become a research hotspot [6–11].

At present, the reported channelized receivers based on microwave photons can be divided into the following three categories. In the first category, each channel independently filters the light waves and then directly detects [12]. A single-carrier or multi-carrier is used to modulate and split or de-multiplex the RF signal into multiple channels. Each channel passes through a fiber Bragg grating (FBG), Fabary–Perot (F-P) cavity, and other filters for direct intensity detection [13,14]. However, this method can only perform intensity detection and cannot extract the RF phase information. In the second category, two optical frequency combs (OFCs) are used as the optical carrier and the optical local oscillator (LO) [15,16], respectively. The RF signal is modulated onto the carrier OFC, and then filtered into multiple channels by the F-P cavity filter. Then the sub-channels coherently detect with the LO OFC to achieve frequency down-conversion [17]. Finally, the IF signals with common frequency are obtained. The disadvantage of this scheme is that it has high requirements on the Q factor and the wavelength stability of the F-P filter. In the third category, uses optical frequency shifter (OFS) to perform a reasonable frequency shift on the LO, and then beats with the modulated RF signal to finally obtain the common intermediate frequency (IF) signals.However, this scheme uses multiple frequency shift signals and the system is more complicated.

In this paper, we bring forward a method for realizing a zero-IF channelized receiver by using a dual polarization quadrature phase shift keying (DP-QPSK) modulator and a narrow-band optical filter bank. The method only needs one optical frequency comb to realize zero-IF multi-channel reception of the wideband signal, and the comb-line interval of the optical-frequency comb only needs to be equal to the sub-channel width, which is easy to implement. Due to the use of photonic I/Q demodulation and balanced detection reception technology, the ADC bandwidth and sampling rate are reduced, and the LO leakage, direct current (DC) offset, even distortion, I/Q imbalance, etc. of the traditional zero-IF receiver are eliminated.

2. Principle

Figure 1 shows the schematic diagram of the proposed microwave photonic channelized receiver with zero-IF architecture. It mainly consists of a laser diode (LD), a DP-QPSK modulator, two LO signals (LO$_1$ and LO$_2$), a set of optical bandpass filters (OBPFs), a single polarization MZM, several polarization controllers (PCs), several polarization beam splitters (PBSs), and several pairs of balanced photodiodes (BPDs).
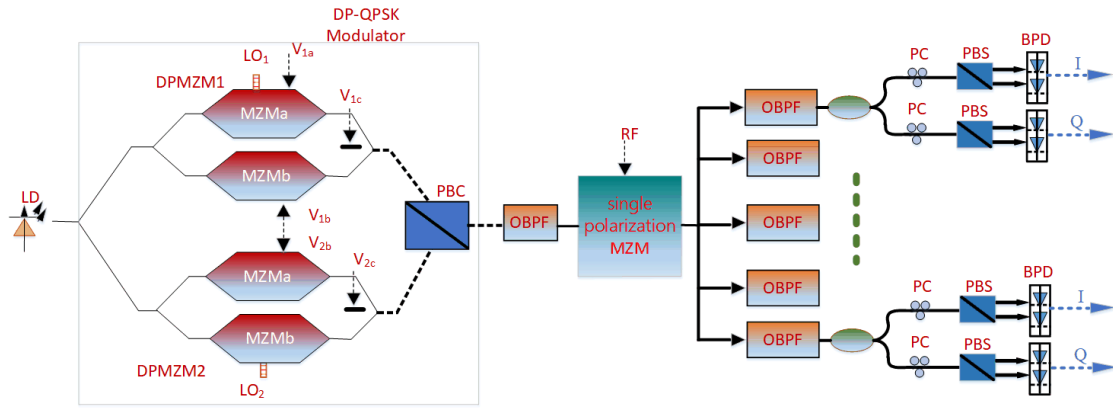
Figure 1. Schematic diagram of proposed microwave photonic channelization receiver with zero-intermediate frequency (IF) architecture, which mainly consists of polarization multiplexed signals generation, photonic microwave in-phase/quadrature (I/Q) mixing, and balanced detection. LD: laser diode; DPMZM: dual parallel Mach–Zehnder modulator; LO: local oscillator; PBC: polarization beam combiner; OBPF: optical bandpass filter; RF: radio frequency; PC: polarization controller; PBS: polarization beam splitter; BPD: balanced photodiode.

In the proposed system, the DP-QPSK modulator is integrated by two parallel DPMZMs (DPMZM1 and DPMZM2) and a polarization beam combiner (PBC). Each DPMZM is composed of two parallel sub-MZMs (MZMa and MZMb) and a main modulator (MZMc). The LD generates a continuous light wave with a frequency of 193.1 THz and a power of 20 dBm, and the continuous light wave is launched into the DP-QPSK modulator as a carrier. Supposing the light wave generated from the LD is expressed as $E_{\text{in}}(t) = E_0 \exp(j\omega_c t)$ where E_0 and ω_c are the amplitude and angular frequency, respectively. After equal power splitting, two light waves are modulated by the LO_1 and LO_2 signals, respectively.

In DPMZM1, only LO_1 signal with a frequency of 0.6 GHz is applied to drive MZMa and a push–pull configuration of the sub-MZMs is assumed. The LO_1 signal can be expressed as $V_{LO1} = V_0 \sin(\omega_{LO1} t)$. V_{1a}, V_{1b}, and V_{1c} represent the three DC bias voltages respectively. The output field of the DPMZM1 can be expressed as [18]:

$$E_{\text{DPMZM1}} = \frac{E_{in}(t)}{2} \left\{ \cos\left[\frac{\pi V_0}{2V_\pi} \sin(\omega_{LO1}t) + \frac{\pi V_{1a}}{2V_\pi}\right] + \cos\left(\frac{\pi V_{1b}}{2V_\pi}\right) e^{j\frac{\pi V_{1c}}{V_\pi}} \right\} \tag{1}$$

where V_π is the half-wave voltage of the modulators. Based on Jacobi–Anger expansion to the output field, the optical carrier, first-order and second-order sidebands can be expressed as follows.

$$E_0 = \frac{E_{in}(t)}{2} \left[\cos A J_0(B) + \cos\left(\frac{\pi V_{1b}}{2V_\pi}\right) e^{j\frac{\pi V_{1c}}{V_\pi}} \right] \tag{2}$$

$$E_{+1} = \frac{E_{in}(t)}{2} \sin A J_1(B) e^{j(\omega_{LO1}t + \frac{\pi}{2})} \tag{3}$$

$$E_{-1} = \frac{E_{in}(t)}{2} \sin A J_1(B) e^{j(\omega_{LO1}t - \frac{\pi}{2})} \tag{4}$$

$$E_{+2} = \frac{E_{in}(t)}{2} \cos A J_2(B) e^{j2\omega_{LO1}t} \tag{5}$$

$$E_{-2} = \frac{E_{in}(t)}{2} \cos A J_2(B) e^{-j2\omega_{LO1}t} \tag{6}$$

where $A = \pi V_{1a}/2V_\pi$, $B = \pi V_0/2V_\pi$, $\omega_{LO1} = 2\pi f$, and $J_n(x)$ represent the nth-order Bessel function. The optical carrier, first-order and second-order sidebands together can form five comb lines. The amplitude of each comb directly affects the flatness of the five comb lines. Therefore, Equations (2)–(6)

can also be regarded as the expression of the five combs. We can see that, if the following equations are satisfied, five flat comb lines can be generated [19]:

$$\frac{E_{in}(t)}{2}\sin A J_1(B) = \frac{E_{in}(t)}{2}\cos A J_2(B) = U \tag{7}$$

$$\frac{E_{in}(t)}{2}\left[\cos A J_0(B) + \cos\left(\frac{\pi V_{1b}}{2V_\pi}\right)e^{j\frac{\pi V_{1c}}{V_\pi}}\right] = -U \tag{8}$$

From Equations (7) and (8), the three DC bias voltages can be expressed:

$$V_{1a} = \frac{2V_\pi}{\pi}\arctan[J_2(B)/J_1(B)] \tag{9}$$

$$V_{1C} = (2N+1)V_\pi, V_{1b} = \frac{2V_\pi}{\pi}\{\pm\arccos[\sin A J_1(B) + \cos A J_0(B)]\} \tag{10}$$

$$V_{1C} = 2NV_\pi, V_{1b} = \frac{2V_\pi}{\pi}\{\pm\arccos[-\sin A J_1(B) - \cos A J_0(B)]\} \tag{11}$$

The half-wave voltage of the MZM is 3.5 V and the modulation index (MI) is 0.83 at this time. From Equations (9)–(11), when the three DC bias voltages of DPMZM1 are V_{1a} = 3.15 V, V_{1b} = −6.23 V, and V_{1c} = 0 V, a five flat comb lines can be generated.

In DPMZM2, only the LO_2 signal with a frequency of 10 GHz and amplitude is 1.4 V is applied to drive MZMb and a push–pull configuration of the sub-MZMs is assumed. The output field of the DPMZM2 can be expressed as:

$$E_{\text{DPMZM2}} = \frac{E_{in}(t)}{2}\left\{\cos\left[\frac{\pi V_{LO2}}{2V_\pi}\sin(\omega_{LO2}t) + \frac{\pi V_{2a}}{2V_\pi}\right] + \cos\left(\frac{\pi V_{2b}}{2V_\pi}\right)e^{j\frac{\pi V_{2c}}{V_\pi}}\right\} \tag{12}$$

$$E_{MZMa} = \frac{E_{in}(t)}{2}\cos\left[\frac{\pi V_{LO2}}{2V_\pi}\sin(\omega_{LO2}t) + \frac{\pi V_{2a}}{2V_\pi}\right] \tag{13}$$

In order to output even-order optical bands, it can be operated at the maximum transmission point (MATP). Therefore, we can get $V_{2a} = 0$, where $A = \pi V_{1a}/2V_\pi$, $B = \pi V_0/2V_\pi$, and $\omega_{LO2} = 2\pi f$. The optical signal output from the MZMa can be rewritten as:

$$E_{MZMa} = \frac{E_{in}(t)}{2}\left[J_0(B) + 2\sum_{n=1}^{\infty} J_{2n}(B)\cos(2n\omega_{LO2}t)\right] \tag{14}$$

In order to suppress the carrier of MZMa to the greatest extent, MZMb is set to work at the minimum transmission point (MITP), finally, the second-order optical bands of carrier suppression are obtained after modulation.

$$E_{MZMb} = \frac{E_{in}(t)}{2}\cos\left(\frac{\pi V_{2b}}{2V_\pi}\right)e^{j\frac{\pi V_{2c}}{V_\pi}} = -\frac{E_{in}(t)}{2}\cos\left(\frac{\pi V_{2b}}{2V_\pi}\right) \tag{15}$$

$$J_0(B) - \frac{E_{in}(t)}{2}\cos\left(\frac{\pi V_{2b}}{2V_\pi}\right) = 0 \tag{16}$$

From Equations (14)–(16), the three DC bias voltages of DPMZM2 are V_{2a} = 0 V, V_{2b} = 0.83 V, and V_{2c} = 0 V. The DPMZM2 outputs positive and negative second-order optical bands with a suppressed carrier. The positive and negative second-order sideband frequencies are −20 GHz and 20 GHz with respect to 193.1 THz, respectively. The output field of DPMZM2 can be expressed as:

$$E_{DPMZM2} = \frac{\sqrt{2}E_{in}(t)}{2}J_2(m_{LO2})[\exp(j2\omega_{LO2}t) + \exp(-j2\omega_{LO2}t)] \tag{17}$$

In brief, Equations (1)–(11) explain the generation of five comb lines, and Equations (12)–(17) explain the generation of second-order optical bands of carrier suppression.

The two optical signals output from DPMZM1 and DPMZM2 are combined by the following PBC, and then they travel out of the DP-QPSK modulator. The combined optical signal can be expressed as:

$$E_{DP-QPSK}(t) = \vec{e}_{TE} \cdot E_{DPMZM1}(t) + \vec{e}_{TM} \cdot E_{DPMZM2}(t) \tag{18}$$

where $\vec{e}_{TE}$ and $\vec{e}_{TM}$ denote the unit vectors of *TE* and *TM* modes, respectively. The optical frequency comb from the DPMZM1 output is in the *TE* mode, and the positive and negative second-order optical sidebands from the DPMZM2 output are in the *TM* mode.

The polarization multiplexed signal output from the DP-QPSK modulator is sent to the OBPF, and the optical frequency comb and the positive second-order optical sideband are filtered out and can be expressed as:

$$E_{OBPF}(t) = \left| \begin{matrix} \frac{E_{in}(t)}{2} \left[\begin{matrix} \cos A J_0(B) + \cos\left(\frac{\pi V_{1b}}{2V_\pi}\right) e^{j\frac{\pi V_{1c}}{V_\pi}} \\ + \sin A J_1(B) e^{j(\omega_{LO1}t + \frac{\pi}{2})} + \sin A J_1(B) e^{j(\omega_{LO1}t - \frac{\pi}{2})} \\ + \cos A J_2(B) e^{j2\omega_{LO1}t} + \cos A J_2(B) e^{-j2\omega_{LO1}t} \end{matrix} \right] \\ \frac{\sqrt{2}E_{in}(t)}{2} J_2(m_{LO2})[\exp(j2\omega_{LO2}t)] \end{matrix} \right| \tag{19}$$

The output port of the OBPF is connected to the single polarization MZM. The wideband RF signal sent to the single polarization MZM consists of five vector signals with a symbol rate of 500 MSym/s and a modulation format of hexadecimal quadrature amplitude modulation (16 QAM) and center frequencies of 18.8 GHz, 19.4 GHz, 20 GHz, 20.6 GHz, and 21.2 GHz, respectively. The RF signal can be expressed as $V_{RF}(t)\sin[\omega_{RF}t + \varphi(t)]$. The wideband RF signal is only modulated by the *TM* mode (positive second-order optical sideband) and is not modulated by the *TE* mode (optical frequency comb). The DC bias of the single-polarized MZM is set to be operated at the MITP to realize the double-side band modulation with carrier suppression. The signal output from the single polarization MZM modulation can be expressed as:

$$\begin{aligned} E_{out} &= \frac{E_{DPMZM2}(t)}{2} \left\{ \begin{matrix} \exp[jm_{RF}\sin(\omega_{RF}t + \varphi(t))] \\ -\exp[-jm_{RF}\sin(\omega_{RF}t + \varphi(t))] \end{matrix} \right\} \\ &= \frac{E_{DPMZM2}(t)}{2} \left\{ \begin{matrix} \sum\limits_{n=-\infty}^{\infty} J_n(m_{RF})\exp[jn(\omega_{RF}t + \varphi(t))] \\ -\sum\limits_{n=-\infty}^{\infty} J_n(m_{RF})\exp[-jn(\omega_{RF}t + \varphi(t))] \end{matrix} \right\} \end{aligned} \tag{20}$$

Since the center frequency of the broadband RF signal is equal to twice the frequency of the LO_2, the center frequency of the lower sideband of the modulated broadband RF signal is equal to the center frequency of the optical frequency comb. The output of the single polarization MZM is divided into five channels by the optical splitter. Each channel passes through the narrowband OBPF with different center frequencies. The center frequencies of the five channels are 193.0988 THz, 193.0994 THz, 193.1 THz, 193.1006 THz, and 193.1012 THz, respectively, and the bandwidth is 600 MHz, which realizes simultaneous segmentation of wideband signals and optical frequency combs.

The following is an example of down-conversion for a sub-channel with the center frequency of 21.2 GHz. The OBPF1 filters out the negative second-order band of the RF signal on the first-line of the optical comb. The sub-RF signal can be expressed as $V_{RF1}(t)\sin[\omega_{RF1}t + \varphi_1(t)]$, and the optical signal output from OBPF1 is expressed as

$$\begin{aligned} E_{OBPF1}(t) &= \left| \begin{matrix} E_{-2}(t) \\ E_{\omega_{RF1}}(t) \end{matrix} \right| \\ &= \frac{E_{in}(t)}{2} \left| \begin{matrix} \cos A J_2(B)\exp(-j2\omega_{LO1}t) \\ \sqrt{2}J_2(m_{LO2})\exp(j2\omega_{LO2}t) \cdot J_1(m_{RF1})\exp[-j(\omega_{RF1}t + \varphi_1(t))] \end{matrix} \right| \end{aligned} \tag{21}$$

An optical splitter can be used to split the optical signal into two channels. Each channel has a PC and a PBS which can generate the following two different optical signals:

$$E_1(t) = \frac{E_{in}(t)}{2} \left\{ \begin{array}{l} \cos A J_2(B) \exp(-j2\omega_{LO1}t) \cos \alpha \\ + \sqrt{2} J_2(m_{LO2}) \exp(j2\omega_{LO2}t) \\ \cdot J_1(m_{RF1}) \exp[-j(\omega_{RF1}t + \varphi_1(t))] \sin \alpha \exp(j\phi) \end{array} \right\} \tag{22}$$

$$E_2(t) = \frac{E_{in}(t)}{2} \left\{ \begin{array}{l} \cos A J_2(B) \exp(-j2\omega_{LO1}t) \sin \alpha \\ - \sqrt{2} J_2(m_{LO2}) \exp(j2\omega_{LO2}t) \\ \cdot J_1(m_{RF1}) \exp[-j(\omega_{RF1}t + \varphi_1(t))] \cos \alpha \exp(j\phi) \end{array} \right\} \tag{23}$$

where α refers to polarization azimuth, and ϕ refers to the phase difference between the two polarization components. To achieve balanced detection, PC is adjusted and $\alpha = 45°$. In the balanced photodiode (BPD), the two photocurrents subtract each other, and the following current is generated after BPD [11]:

$$i(t) \propto |E_1(t)|^2 - |E_2(t)|^2 \propto$$
$$\cos A J_2(B) J_2(m_{LO2}) J_1(m_{RF1}) \cos[(-2\omega_{LO1} - 2\omega_{LO2} + \omega_{RF1})t - 2\varphi_1(t) - \phi] \tag{24}$$

The main purpose of usingbalanced detection is to supress even-order distortion and eliminate DC offset. Since the phase of the baseband signal is related to ϕ, which can be arbitrarily tuned through polarization control.

In the first channel, the PC is adjusted to set $\phi = 0°$, and the photocurrent after BPD can be written as:

$$i_I(t) \propto \cos A J_2(B) J_2(m_{LO2}) J_1(m_{RF1}) \cos[(-2\omega_{LO1} - 2\omega_{LO2} + \omega_{RF1})t - 2\varphi_1(t)] \tag{25}$$

Thus, an in-phase down-converted IF signal is obtained.

In the other channel, the PC is adjusted to set $\varphi = 90°$, and the photocurrent after BPD can be written as:

$$i_Q(t) \propto \cos A J_2(B) J_2(m_{LO2}) J_1(m_{RF1}) \sin[(-2\omega_{LO1} - 2\omega_{LO2} + \omega_{RF1})t - 2\varphi_1(t)] \tag{26}$$

The two PCs are adjusted so that the phase difference between one optical carrier and the RF signal is 0°, so that the channel information outputs after passing through the PBS and the BPD. The phase difference between the other optical carrier and the RF signal is 90°, so the Q channel information outputs after passing through the PBS and the BPD. The five channels in parallel are identical after the narrowband OBPF. Therefore, the five sub-IF signals output from each channel is sent to the ADC for electrical domain signal processing. The parameters used in the simulation are shown in Table 1.

Table 1. The main parameters of the building blocks used in the Virtual Photonic incorporation (VPI) simulation.

| Component	Parameters
LD	power of 10 dBm; linewidth 1 kHz; relative intensity noise (RIN) of -160 dB
LO_1	amplitude of 10 dBm; frequency 0.6 G
DPMZM1	insertion loss of 6 dB; $V_\pi = 3.5$ V; $V_{1a} = 3.15$ V; $V_{1b} = -6.23$ V; $V_{1c} = 0$ V
LO_2	amplitude of 8 dBm; frequency 10 G
DPMZM2	insertion loss of 6 dB; $V_\pi = 3.5$ V; $V_{2a} = 0$ V; $V_{2b} = 0.83$ V; $V_{2c} = 0$ V
OBPF	center frequency of 20 G; bandwidth of 30 G
MZM	insertion loss of 6 dB; $V_\pi = 3.5$ V; $V_{dc} = 1.75$ V;
narrowband OBPFs	center frequencies of 18.8 GHz, 19.4 GHz, 20 GHz, 20.6 GHz, and 21.2 GHz, respectively; bandwidth of 600 M

3. Results and Discussion

3.1. Generation of Polarization Multiplexed Signals

The proposed system was simulated by VPItransmissionMaker software. The half-wave voltage of MZM was 3.5 V. The extinction ratio was 30 dB and the insertion loss was 6 dB. A continuous wave light was launched into DPMZM1 and DPMZM2 in parallel, with a frequency of 193.1 THz, an average power of 20 dBm, a linewidth of 10 kHz, and a maximum relative intensity noise (RIN) of −170 dB/Hz. DPMZM1 output five flat line combs with a frequency spacing of 0.6 GHz. The frequencies of the optical comb were −1.2 GHz, −0.6 GHz, 0 GHz, 0.6 GHz, and 1.2 GHz, respectively, relative to 193.1 THz. Figure 2 shows five flat comb lines with nearly the same amplitude. The unwanted mode suppression ratio (UMSR) was 23.3 dB.
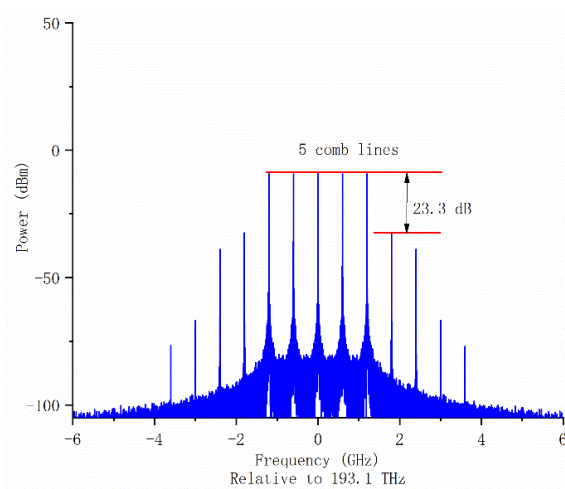
Figure 2. The spectrum modulated by DPMZM1.

As is shown in Figure 3, DPMZM2 output carrier-suppressed positive and negative second-order optical sidebands, and the frequencies of positive and negative second-order sidebands were −20 GHz and 20 GHz, respectively, relative to 193.1 THz. The UMSR was 35.6 dB.
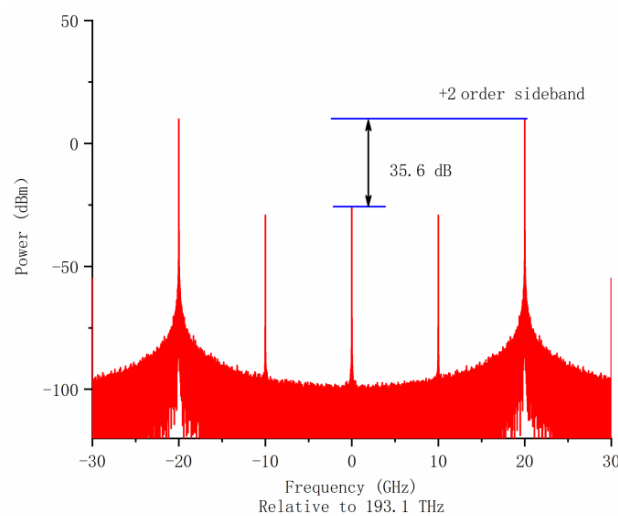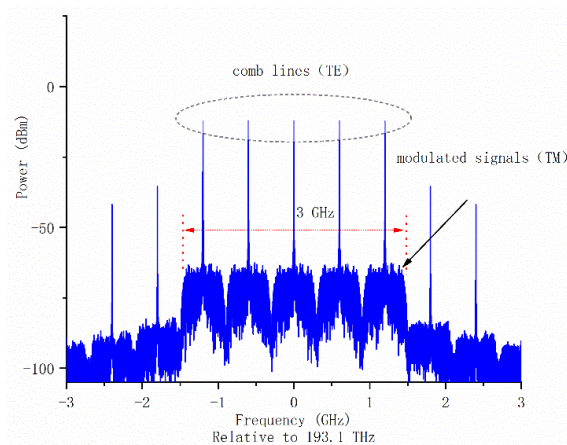

Figure 3. The spectrum modulated by DPMZM2.

The polarization multiplexed signal output from the DP-QPSK modulator was sent to the OBPF, and the optical frequency comb and the positive second-order optical sideband were filtered out. The

optical frequency comb from the DPMZM1 was combed in the *TE* mode, and the positive and negative second-order optical sidebands from the DPMZM2 were in the *TM* mode. The output port of the OBPF was connected to a single polarization MZM. The five-symbol rate was 500 MSym/s and the modulation format was 16 quadrature amplitude modulation (16 QAM). The vector signals with center frequencies of 18.8 GHz, 19.4 GHz, 20 GHz, 20.6 GHz, and 21.2 GHz formed a wideband RF signal. The wideband RF signal was modulated in a single polarization MZM only in the *TM* mode (positive second-order optical sideband) and not modulated in the *TE* mode (optical frequency comb). The DC bias of the single-polarized MZM was set to MITP to achieve double-band modulation with carrier suppression. As shown in Figure 4, since the center frequency of the broadband RF signal is equal to twice the LO_2 frequency, the center frequency of the lower sideband of the modulated broadband RF signal coincides with the center frequency of the optical frequency comb.

Figure 4. The spectrum modulated by the wideband RF signals.

The output of the single-polarized MZM was divided into five channels by an optical splitter, each passing through a narrow-band OBPF with different center frequencies. The center frequencies of the five channel filters were 193.0988 THz, 193.0994 THz, 193.1 THz, 193.1006 THz, and 193.110 THz, respectively. The polarization multiplexed light output from each narrowband OBPF included an optical carrier (one of the five comb lines) and a sub-channel RF signal, as shown in Figure 5, realizing the band division of the 3 GHz wideband signal. The frequency of the optical carrier was equal to the center frequency of the RF sub-channel, and the bandwidth of the five channels was 600 MHz.
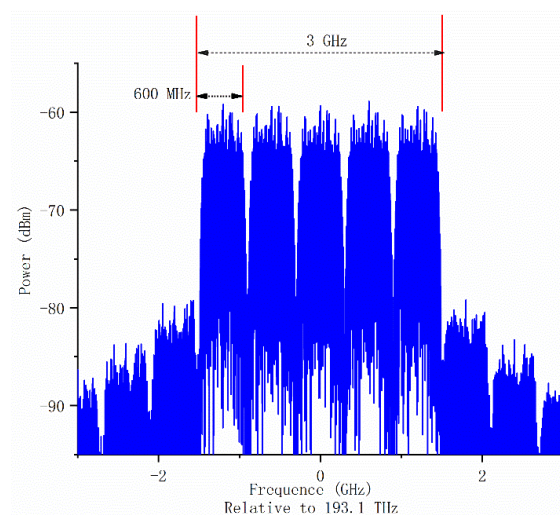
Figure 5. Five subchannels with a bandwidth of 600 HMz.

3.2. Balanced Detection and IQ Demodulation

The output optical signal of the narrowband OBPF passed through a 1:2 optical splitter, and the upper and lower parts were connected to two BPDs through PCs and PBSs. By adjusting the two PCs, the phase difference between the optical carrier and the RF signal was 0°, and the in-phase channel information was then obtained after passing through the PBS and BPD. The phase difference between the other optical carrier and the RF signal was 90°, so that the quadrature channel information was obtained after passing through the PBS and BPD.

Balanced detection can effectively suppress the common mode interference (mainly including second-order intermodulation distortions (IMD2) and DC terms). In order to demonstrate the distortion suppression and linearization ability, two-tone signals with frequencies of 21 and 21.01 GHz and the powers of 0 dBm were used as the input RF signal.

Figure 6a shows the results without balanced detection, where a conversion gain of −41.2 dB, a noise figure (NF) of 53.1 dB, and a third-order input intercept point (IIP3) were obtained. Although the third-order spurious free dynamic range (SFDR3) reached 106.7·dB·Hz2/3, the second-order intermodulation distortions (IMD2) were always the dominant distortion and dragged the second-order SFDR (SFDR2) to only 76.5 dB·Hz1/2, which determined the overall SFDR of the system. Figure 6b shows the results with balanced detection, the conversion gain was −35.2 dB, where the 6 dB improvement benefits from the balanced detection. The NF with balanced detection was measured to 50.1 dB and the SFDR was 107.5 dB·Hz2/3, which also improved compared to those without balanced detection. What is more important, since the simulation is performed under ideal conditions, the comparison between the two shows that the balance detection can theoretically completely cancel the IMD2. Figure 7 shows the spectra of the I and Q electrical signals obtained by balanced detection. The bandwidth of the I and Q baseband signals was 300 MHz, which is half of the bandwidth of the RF signal. Thanks to the balanced detection, no obvious distortion and DC terms were observed.
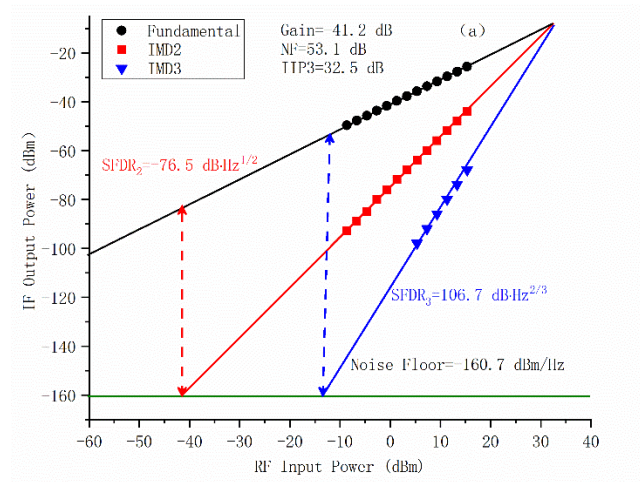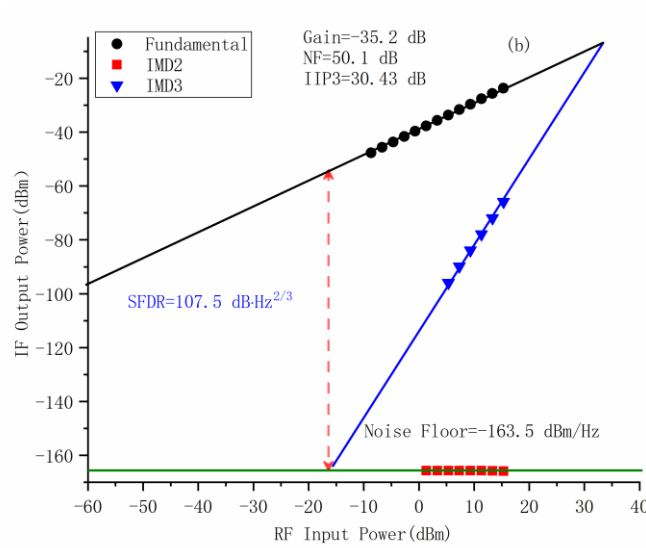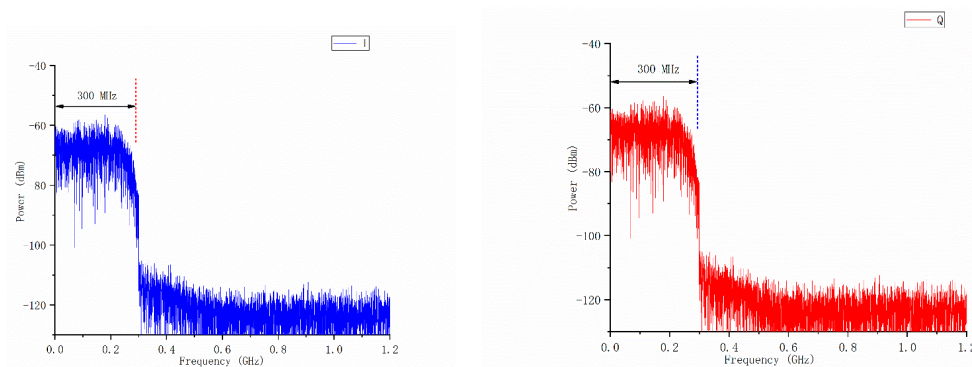
Figure 6. *Cont.*

Figure 6. Measured powers of fundamental term, second-order intermodulation distortions (IMD2), third-order intermodulation distortions (IMD3), and noise floor in output IF signals as a function of RF input power. (**a**) Without balanced detection; (**b**) with balanced detection. Two-tone RF frequencies: 21 and 21.01 GHz. LO frequency: 20.9 GHz. RF power: 0 dBm.


Figure 7. Measured I and Q spectrum with balanced detection.

Channel crosstalk is mainly caused by the residual optical carrier and sidebands. In order to get simulation results that agree with practical applications, the extinction ratio of the MZMs in the simulation was set to 30 dB. The channel crosstalk was tested and is shown in Table 2. We can see the channel isolations are all over 25 dB.

Table 2. Measured channel crosstalk between all sub-channels.

Sub-Channel	1	2	3	4	5
1	0	25.5 dB	26.5 dB	27.5 dB	28.5 dB
2	25.5 dB	0	25.5 dB	26.5 dB	27.5 dB
3	26.5 dB	25.5 dB	0	25.5 dB	26.5 dB
4	27.5 dB	26.5 dB	25.5 dB	0	25.5 dB
5	28.5 dB	27.5 dB	26.5 dB	25.5 dB	0

Figure 8 shows the simulated error vector magnitude (EVM) curves and constellation diagrams when the power of the RF signal is tuned from −20 to 20 dBm. We can see clearly that when the RF power increases, With the increase of RF power, EVM will decline steadily and eventually stabilize at 1,7%. Especially when the RF input power is greater than -5dB, the EVM will drop below 10%, indicating that the system has a considerable dynamic range under these conditions.
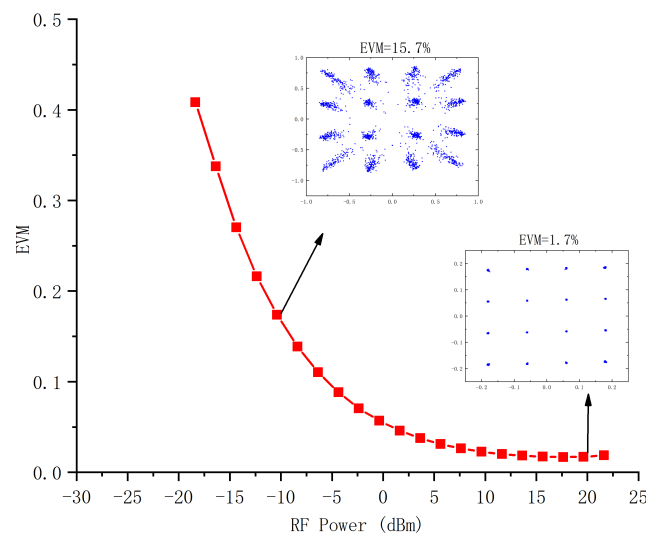
Figure 8. Measured error vector magnitude (EVM) and constellation diagram when the power of the RF signal is tuned from −20 to 20 dBm. Modulation format: 16 QAM; signal bandwidth: 600 MBand.

4. Conclusions

An ultra-wideband photonic microwave channelization for a zero-IF receiver was proposed and demonstrated by simulation in this paper. Owing to all-optical techniques and I/Q balanced detection, it exhibited advantages including ultra-wide operating band, low conversion loss, accurate I/Q amplitude and phase balance, and large dynamic range. Meanwhile, due to balanced detection, the DC offset and IMD2 were well suppressed. Simulation results show that the RF signal with a bandwidth of 3 GHz can be divided into five sub-channels with a bandwidth of 600 MHz. The measured SFDR was 107.5 dB·Hz2/3. The scheme only needs a set of optical frequency combs and narrowband OBPF group to realize channelization processing of wideband signals, and can also be applied to analog radio over fiber transmissions in uplink communications [20,21].

Author Contributions: B.C. and Y.G. conceived and designed the experiments. B.C. performed the experiments. B.C. and Y.F. analyzed the data. B.C. wrote the article. W.W. and B.K. reviewed and edited the manuscript. B.C., Z.T., and W.J. responded to the reviews and revised the manuscript. All authors have read and agreed to the published version of the manuscript.

Conflicts of Interest: The authors declare no conflicts of interest.

References

1. Sevenhans, J.; Verstraeten, B.; Taraborrelli, T. Trends in silicon radio large scale integration: Zero IF receiver! Zero I&Q transmitter! Zero discrete passives! *IEEE Commun. Mag.* **2000**, *38*, 142–147.
2. Nakazawa, M.; Hirooka, T.; Ruan, P.; Guan, P. Ultrahigh-speed "orthogonal" TDM transmission with an optical Nyquist pulse train. *Opt. Express* **2012**, *20*, 1129–1140. [CrossRef] [PubMed]
3. Hirooka, T.; Nakazawa, M. Linear and nonlinear propagation of optical Nyquist pulses in fibers. *Opt. Express* **2012**, *20*, 19836–19849. [CrossRef] [PubMed]
4. Wang, Q.; Huo, L.; Xing, Y.; Zhou, B. Ultra-flat optical frequency comb generator using a single-driven dual-parallel Mach-Zehnder modulator. *Opt. Lett.* **2014**, *39*, 3050–3053. [CrossRef] [PubMed]

5. Wang, L.X.; Zhu, N.H.; Li, W.; Wang, H.; Zheng, J.Y.; Liu, J.G. Polarization division multiplexed photonic radio-frequency channelizer using an optical comb. *Opt. Commun.* **2013**, *286*, 282–287. [CrossRef]

6. Wang, J.J.; Chen, M.H.; Liang, Y.H.; Chen, H.W.; Yang, S.G.; Xie, S.Z. Broadband RF front-end using microwave photonics filter. *Opt. Express* **2015**, *23*, 839–845. [CrossRef] [PubMed]

7. Tang, Z.; Pan, S. Image-reject mixer with large suppression of mixing spurs based on a photonic microwave phase shifter. *J. Lightwave Technol.* **2016**, *34*, 4729–4735. [CrossRef]

8. Yang, X.W.; Xu, K.; Yin, J.; Dai, Y.T.; Yin, F.F.; Li, J.Q.; Lu, H.; Liu, T. Optical frequency comb based multi-band microwave frequency conversion for satellite applications. *Opt. Express* **2014**, *22*, 869–877. [CrossRef] [PubMed]

9. Tang, Z.Z.; Zhu, D.; Pan, S.L. Coherent optical RF channelizer with large instantaneous bandwidth and large in-band interference suppression. *J. Lightwave Technol.* **2018**, *36*, 4219–4226. [CrossRef]

10. Gao, Y.S.; Wen, A.J.; Zhang, W.; Jiang, W.; Ge, J.H.; Fan, Y.Y. Ultra-wideband photonic microwave I/Q mixer for zero-IF receiver. *IEEE Trans. Microw. Theory Tech.* **2017**, *65*, 4513–4525. [CrossRef]

11. Gao, Y.S.; Wen, A.J.; Jiang, W.; Fan, Y.Y. All-optical and broadband microwave fundamental/sub-harmonic I/Q down-converters. *Opt. Express* **2018**, *26*, 7336–7350. [CrossRef] [PubMed]

12. Tang, Z.Z.; Pan, S.L. A reconfigurable photonic microwave mixer using a 90° optical hybrid. *IEEE Trans. Microw. Theory Tech.* **2016**, *64*, 3017–3025. [CrossRef]

13. Tang, Z.; Zhang, F.; Pan, S.L. Photonic microwave downcon-verter based on an optoelectronic oscillator using a single dual-drive Mach–Zehnder modulator. *Opt. Express* **2014**, *22*, 305–310. [CrossRef] [PubMed]

14. Gao, Y.S.; Wen, A.J.; Wu, X.; Wang, Y.; Zhang, H. Efficient photonic microwave mixer with compensation of the chromatic dispersion-induced power fading. *J. Lightwave Technol.* **2016**, *34*, 3440–3448. [CrossRef]

15. Pagán, V.R.; Murphy, T.E. Electro-optic millimeter-wave harmonic downconversion and vector demodulation using cascaded phase modulation and optical filtering. *Opt. Lett.* **2015**, *40*, 2481–2484. [CrossRef] [PubMed]

16. Zou, X.; Lu, B.; Pan, W.; Yan, L.; Stöhr, A.; Yao, J. Photonics for microwave measurements. *Laser Photonics Rev.* **2016**, *10*, 711–734. [CrossRef]

17. Jiang, W.; Zhao, S.H.; Tan, Q.G.; Liang, D.; Li, X.J.; Gao, Y.S. Wideband photonic microwave channelization and image-reject down-conversion. *Opt. Commun.* **2019**, *445*, 41–49. [CrossRef]

18. Li, Y.; Wu, J.; Yu, J.; Kong, D.M.; Li, W. Generation and performance Investigation of 40GHz phase stable and pulse width-tunable optical time window based on a DPMZM. *Opt. Express* **2012**, *20*, 24754–24760.

19. Wu, J.; Zang, J.Z.; Li, Y.; Kong, D.M.; Qiu, J.F. Investigation on Nyquist pulse generation using a single dual-parallel Mach-Zehnder modulator. *Opt. Express* **2014**, *22*, 20463–20472. [CrossRef] [PubMed]

20. Vagionas, C.; Papaioannou, S.; Kalfas, G.; Pleros, N. A six-channel mmWave/IFoF link with 24Gb/s capacity for 5G fronthaul networks. In Proceedings of the 2018 International Topical Meeting on Microwave Photonics (MWP), Toulouse, France, 22–25 October 2018.

21. Kalfas, G.; Vagionas, C.; Antonopoulos, A.; Kartsakli, E. Next generation Fiber-Wireless fronthaul for 5G mmWave networks. *IEEE Commun. Mag.* **2019**, *57*, 138–144. [CrossRef]